Physics – Uspekhi **56** (1) 79 – 92 (2013)

PHYSICS OF OUR DAYS

PACS numbers: 47.15.G –, 47.57.J –, 47.63.Gd, 64.75.Yz, 81.05Xj

Active colloids

I S Aranson

DOI: 10.3367/UFNe.0183.201301e.0087

Contents

Abstract. A colloidal suspension is a heterogeneous fluid containing solid microscopic particles. Colloids play an important role in our everyday life, from food and pharmaceutical industries to medicine and nanotechnology. It is useful to distinguish two major classes of colloidal suspensions: equilibrium and active, i.e., maintained out of thermodynamic equilibrium by external electric or magnetic fields, light, chemical reactions, or hydrodynamic shear flow. While the properties of equilibrium colloidal suspensions are fairly well understood, active colloids pose a formidable challenge, and the research is in its early exploratory stage. One of the most remarkable properties of active colloids is the possibility of dynamic self-assembly, a natural tendency of simple building blocks to organize into complex functional architectures. Examples range from tunable, self-healing colloidal crystals and membranes to self-assembled microswimmers and robots. Active colloidal suspensions may exhibit material properties not present in their equilibrium counterparts, e.g., reduced viscosity and enhanced self-diffusivity, etc. This study surveys the most recent developments in the physics of active colloids, both in synthetic and living systems, with the aim of elucidation of the fundamental physical mechanisms governing self-assembly and collective behavior.

I S Aranson Materials Science Division, Argonne National Laboratory, 9700 South Cass Avenue, Argonne, Illinois 60439, USA;
Department of Engineering Sciences and Applied Mathematics, Northwestern University, 2145 Sheridan Rd, Evanston, IL 60208, USA
E-mail: aronson@anl.gov

Received 17 July 2012, revised 2 October 2012
Uspekhi Fizicheskikh Nauk **183** (1) 87 – 102 (2013)
DOI: 10.3367/UFNr.0183.201301e.0087
Translated by the author; edited by M S Aksent'eva

1. Introduction

Colloids are substances consisting of macroscopic particles larger than atoms or molecules, typically from 10 nm to 100 μm, dispersed in another continuum phase, such as liquid or gas [1]. Colloids play an important role in our everyday life (e.g., milk, pigmented ink, blood) and are critical to many industries, from food, pharmaceutical, and medicine to nanotechnology [2] and electronics (colloidal pigment particles are used in low power consumption electrophoretic displays for e-readers [3]). The cross-disciplinary field of colloidal suspensions is an active area of research. Colloidal physics is an important part of 'soft matter', a rapidly expanding field of contemporary science dealing with physical states easily deformable by thermal stresses, fluctuations, or external forces. The scope of soft matter includes colloids, polymers, foams, gels, granular materials, and some biological materials, like suspensions of motile microorganisms (for recent reviews, see [4–9]).

A multitude of forces governs interactions between colloidal particles, like steric repulsion, electrostatic and magnetic forces (for magnetic colloids), van der Waals forces due to electric dipole moments of colloidal particles, gravity, entropic forces, and hydrodynamic and other forces due to the gradients of the surfactant, etc. [9]. Under various experimental conditions, interacting colloidal particles may form a variety of steady states, from colloidal glasses [10] and gels [11] to highly ordered colloidal crystals [12]. Ordered colloidal suspensions find application as optical materials with a photonic band gap [13, 14] (see Fig. 1 in Section 2).

It is important to emphasize the connections between colloids and the related concept of metamaterials. The 20th century saw remarkable progress based on our understanding of hard materials at the atomic level. Only recently did the concept of metamaterials emerge: human-made materials with artificial building units. Metamaterials were conceived, for example, to control the propagation of waves [15] or vary opto-mechanical properties [16]. New functionalities of

metamaterials, such as a negative index of refraction or optical band gap, result from preprogrammed features of artificial meta-atoms. Functionalized colloidal particles, playing the role of meta-atoms, offer a promising platform for the design of metamaterials via controlled and flexible bottom-up assembly.

There is a significant body of work dedicated to various aspects of mostly equilibrium colloidal structures obtained as a result of static self-assembly [17–30]. Some examples of ordered structures, like photonic band gap crystals and ionic colloidal crystals, obtained by equilibrium self-assembly, are shown in Fig. 1a–d in Section 2.

The purpose of this study is to survey recent progress in active (or driven) colloidal systems, both living and synthetic, where formation of dynamic structures occurs under out-of-equilibrium conditions. In particular, actively self-assembled colloidal structures offer new functionalities not available under equilibrium conditions: an ability of self-propulsion [31–33], self-repair [34, 35], manipulation of cargo particles [36], and other functions usually associated with living systems [37]. While active colloids is a rapidly expanding field, there are only a few reviews on this subject [38–40], especially from the point of view of physics.

It is natural to classify collective motion in active colloidal systems according to the way how the energy is injected. One large class is represented by systems driven by external fields, such as electric and magnetic fields, or by hydrodynamic flows. In this situation, the external field exerts forces or torques on the colloidal particles, either in the bulk or at the liquid/solid or liquid/liquid interface. In the second case, the particles are driven internally, for example, by chemical reactions, ultraviolet light, etc. (see, e.g., [41]). Consequently, no net external force is applied to the particle, and the particle is propelled due to the generation of local force dipoles [42]. A large group of self-propelled particles, such as bimetallic chemical microswimmers, asymmetric Janus particles (named after the two-faced Roman god), and even a majority of swimming microorganisms, belongs to this class [43]. It was recently shown by the example of motile bacteria that a suspension of active swimmers may exhibit material properties different from their equilibrium counterpart: a sevenfold reduction of viscosity [44], a dramatic increase in diffusivity [45, 46], etc. It remains a major challenge, however, to obtain similar effects with suspensions of synthetic swimmers.

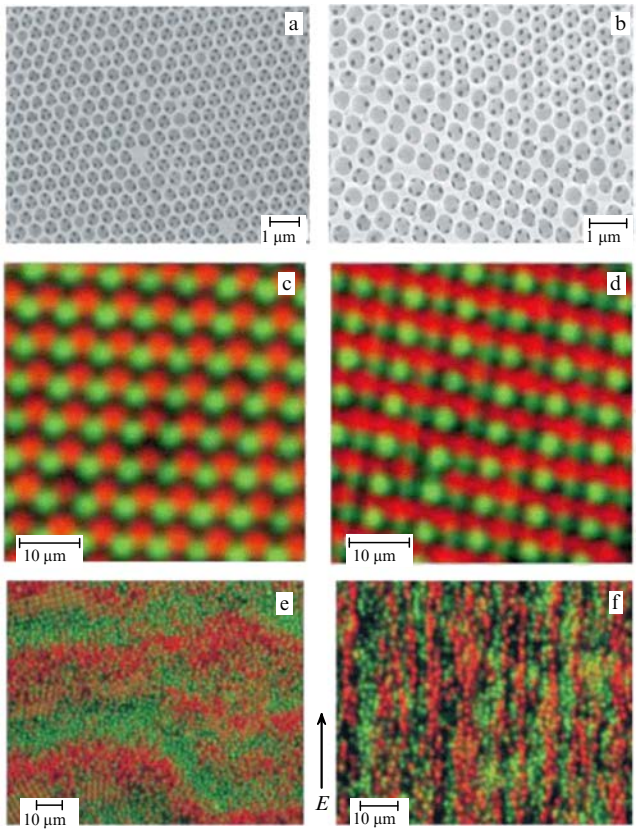

Figure 1. (Color online.) Illustrations of self-assembled colloidal structures. (a) Highly ordered regions with hexagonal symmetry extending over 10 μm assembled from functionalized (patchy) colloidal silica particles. The colloidal structure exhibits a photonic band gap in the visible light range. (b) Regions showing co-existing hexagonal and square symmetry, from [13]. (c, d) Confocal microscope images illustrating highly-ordered self-assembled structures in 'ionic' colloidal crystals of oppositely charged particles assembled from positive (red, 1.08 μm) and negative (green, 0.99 μm) polymethylmethacrylate spheres. (e, f) Electric field E induced structures in the same system: stationary bands perpendicular to the field directions (e) and lanes of oppositely moving particles parallel to the field direction, emerging for larger amplitudes of the applied electric field (f). (Reproduced with the kind permission of the authors of [20, 47] and the Nature Publishing Group).

2. Collective behavior of externally-driven colloidal systems

In this section, we consider large-scale collective states emerging when the colloidal systems are driven by external fields: electric or magnetic. Figures 1–5 illustrate representative self-assembled states observed in this broad class of systems, from nonequilibrium steady-state patterns, like separated bands, lanes, and self-healing membranes [35, 47] to dynamic structures: rotating binary vortices, pulsating rings [48], and self-assembled microswimmers [33].

2.1 Electrostatically-driven colloidal systems

It appears rather challenging to classify patterns and collective behavior emerging in externally driven colloidal systems. For example, in a colloidal system energized by an electric field, the outcome of self-assembly is very sensitive to the amplitude, frequency of the electric field, properties of the suspending fluid (e.g., viscosity, conductivity), and the size, composition, and material properties of the colloidal particles. A system of oppositely-charged colloidal particles in an aqueous solution subject to a low frequency ac electric field segregates into bands perpendicular to the applied field direction [47] (Fig. 1e). The bands disintegrate due to the particles' Brownian diffusion once the field is switched off. The authors of [47] argue that the band formation is caused by collisions between particles moving in opposite directions.

In a similar system of oppositely charged colloids, but under slightly different conditions (a dc electric field of higher magnitude), instead of the static bands formed perpendicular to the field, a phenomenon of the formation of lanes is observed (Fig. 1f). Lanes are stripes formed by particles of opposite polarity and moving in opposite directions, like cars on a two-way highway. In contrast to the static bands, lanes are aligned parallel to the applied field [18]. The authors [18] suggest that the dynamic mechanism responsible for the formation of the lanes is an enhanced lateral mobility of particles induced by collisions with particles driven in the opposite direction. Once the lanes are formed, a particle's

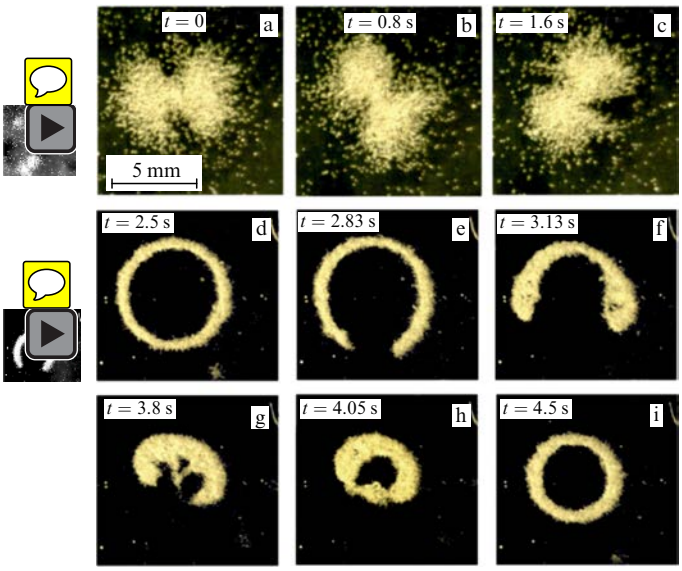

Figure 2. (Color and animation online.) Dynamically self-assembled structures formed by conducting microparticles (100-μm bronze spheres) in a weakly-conducting nonpolar liquid (toluene/alcohol mixture) in a dc electric field. Snapshots (a–c) show rotating binary star-like vortices. Each vortex excites toroidal electroosmotic flow in the suspending liquid (movie 2.1). Upon direction reversal of the electric field, the rotating 'binary stars' transform into pulsating rings (d–i) (movie 2.2). (From [48].)

mobility is sharply decreased. The authors argue that the particles in a lane can be regarded as being in a dynamically 'locked-in' state. For a review of various instabilities in oppositely charged colloidal systems, see [49].

Fascinating dynamically self-assembled structures emerge when conducting microspheres (100-μm bronze particles) are suspended in a thin layer of weakly conducting liquid (toluene/alcohol mixture) and energized by a strong dc electric field (up to 2–3 kV mm^{-1}) [48].[1] Some of these states are shown in Fig. 2. Depending on the amplitude of the dc electric field, its direction with respect to gravity, and alcohol to toluene ratio, a large variety of self-assembled structures is observed. For relatively low applied field values and low alcohol concentration, the patterns are mostly static: clusters, colloidal crystals, or honeycomb lattices. For higher applied field values and higher alcohol concentrations, the static patterns give way to dynamic states, like self-assembled rotating binary star-like vortices (Fig. 2a–c). Upon polarity reversal of the applied electric field, the rotating vortices transform into chaotically pulsating rings (Fig. 2d–i). The primary mechanisms responsible for the interactions between the particles are electrophoresis, i.e., the transport of charged particles by the electric field in the liquid, and electroosmosis, the transport of liquid by the electric field. While toluene is a nonpolar nonconducting fluid, the presence of alcohol makes the mixture a weak ionic conductor due to the small dissociation of the alcohol molecules. For typical experimental conditions (a few percent of alcohol in toluene), the corresponding Debye length is above 1–10 μm, i.e., many orders of magnitude higher than that in water. As a result, the static electric field in the mixture is practically unscreened, making it very different from the colloidal experiments in aqueous solutions [18, 49], where the Debye length is very short — on the order of 10 nm. The electric field causes motion of ions in the bulk of the liquid. Due to the presence of macroscopic conducting particles in the liquid, the flow of the ions is perturbed, resulting in the creation of toroidal electroosmotic flows in the proximity of the particles [48, 51]. The electrophoretic flows, together with the electrostatic interactions between the particles and gravity, are responsible for the creation of dynamic states in the experiment. A phenomenological theory of pattern formation in this system was developed in [52]. Experiments conducted with much smaller particles (2–3-μm gold spheres) revealed, in addition to vortices, dynamically self-assembled wires formed along the field direction and assembling/reassembling tree-like structures [53].

[1] A conducting particle in a contact with conducting plane acquires electric charge by direct electrification. It detaches from the plane and moves upwards if the electric force $F_e = \kappa a^2 E^2$ exceeds the force of gravity, $F_g = 4/3\pi\rho g a^3$, here a is the radius of the particle, E is applied dc vertical electric field, g is acceleration of gravity, ρ is the mass density of the particles, and κ is a constant dependent on the particle shape. For a conducting spherical particle one derives $\kappa = \zeta(3) + 1/3 \approx 1.36$, where ζ is Riemann ζ-function [50].

2.2 Colloidal systems energized by alternating magnetic fields

If colloidal particles possess a magnetic moment, either permanent (ferromagnetic) or induced (superparamagnetic), the self-assembly can be tuned and directed by an external magnetic field. A static field induces either chain-like clusters or bulk colloidal crystals [54]. In contrast, a variety of complex self-assembled structures can form in an alternating magnetic field, from quasi-static sheets and membranes [35] to dynamic self-assembled swimmers [33]. The applied magnetic field can be uniaxial [33], biaxial, or triaxial [35, 55].

Spectacular self-assembled structures emerge when a dispersion of ferromagnetic microparticles (100-μm nickel spheres) is suspended at the water–air interface and energized by an external ac magnetic field $H = H_0 \sin(2\pi f t)$, applied perpendicular to the interface (Fig. 3). Depending on the frequency f and amplitude H_0 of the external magnetic field, the particles self-assemble into linear snake-like objects

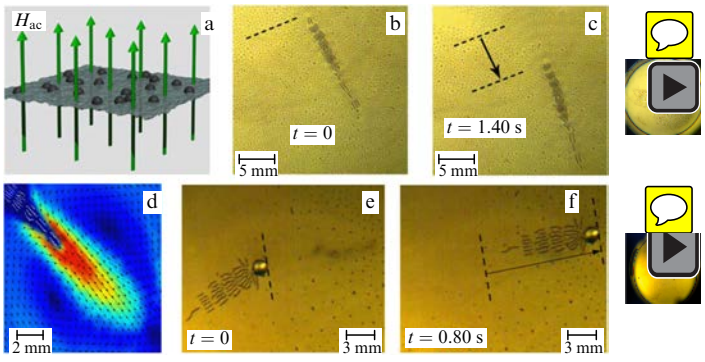

Figure 3. (Color and animation online.) Self-assembled surface swimmer (magnetic snake) formed by ferromagnetic microparticles (80–100-μm nickel spheres) at the water–air interface (a). Schematics of the experiment: a homogeneous ac magnetic field (60–80 Hz), applied perpendicular to the air/water interface, energizes suspended ferromagnetic particles. Images (b, c) illustrate the self-assembled swimmer (magnetic snake) formed spontaneously from a random dispersion of ferromagnetic particles (movie 3.1). (d) A large-scale streaming vortex flow generated by the tail of a magnetic snake; arrows show streamlines, and colors indicate the magnitude of the surface velocity (movie 3.2). (e, f) A swimmer formed by a snake attached to a 1-mm nonmagnetic glass bead (movie 3.3) [33].

(magnetic snakes) (Fig. 3b, c). The snakes are composed of several parallel ferromagnetically-aligned chains (segments). The segments, however, have an anti-ferromagnetic alignment. The distance between the neighboring segments λ is controlled by the frequency of the applied field, while the snake's width W is determined by the field's amplitude. A good approximation for the distance λ as a function of frequency of applied magnetic field f is given by the dispersion relation for gravity-capillary waves on the surface of a deep liquid:

$$f^2 \approx \frac{g}{2\pi\lambda} + \frac{2\pi\sigma}{\rho\lambda^3}\,, \tag{1}$$

where g is the acceleration of gravity, σ is the surface tension, and ρ is the density of the liquid. Thus, the primary mechanism of snake formation is an interplay between particles' magnetic dipolar interaction promoting chain formation and hydrodynamic surface flows excited by the oscillating chains at the air–water interface.

The snakes are immobile for low frequencies f of the field and become self-propelled objects for higher frequencies [33]. Due to the inertia of the fluid, the tails of a snake excite large-scale rectified streaming vortex flows [56], each tail serving as a powerful self-assembled pump (Fig. 3d) (compare to the Rayleigh or acoustic streaming phenomenon [57]). The magnitude of the rectified flow is proportional to H_0^2 and increases roughly linearly with the frequency f. While for relatively low frequencies of the applied field (below 60 Hz) the snake's large-scale flow is symmetric and the snake is immobile, for higher frequencies the symmetry of the flow becomes spontaneously broken, resulting in self-propulsion of the snake (Fig. 3b, c). Apparently, this mechanism of self-propulsion does not have a direct analog in nature. In addition, the symmetry of the snake's large-scale flows can be broken artificially, by placing a large nonmagnetic bead in the proximity of one of the snake's tails. The bead weakens the flow generated by the tail, resulting in an asymmetry of the streaming flow. In this case, the snake attaches to the bead and is propelled by a remaining free tail (Fig. 3e, f). Many aspects of dynamic self-assembly in this system are captured in the framework of a first-principle model based on the particle dynamics coupled to surface deformations in a thin liquid layer [58].

A rich variety of dynamic self-assembled patterns is observed when ferromagnetic microparticles are placed at the interface between two nonmiscible liquids, e.g., silicone oil and water. In this situation, the distance λ is determined by the density difference between two liquids [compare to Eqn (1)],

$$f^2 \approx \frac{g(\rho_1-\rho_2)}{2\pi\lambda(\rho_1+\rho_2)} + \frac{2\pi\sigma_{12}}{(\rho_1+\rho_2)\,\lambda^3}\,, \tag{2}$$

where $\rho_{1,2}$ are the densities of the bottom (1) and top (2) liquids, and σ_{12} is the interfacial tension.[2] Thus, by reducing the density contrast between the liquids $\rho_1-\rho_2$ or the interfacial tension σ_{12}, one can decrease the size of self-assembled snakes λ.

[2] To avoid the Rayleigh–Taylor instability of an interface between two liquids of different densities, the bottom liquid should be heavier than the top one [59].

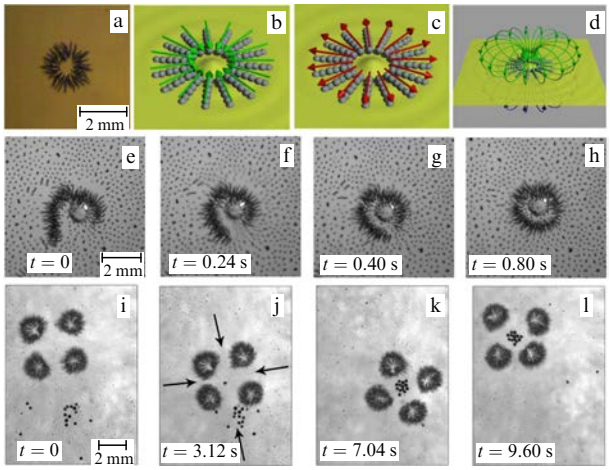

Figure 4. (Color and animation online.) Self-assembled colloidal structures at the interface between two nonmiscible liquids (silicone oil/water). (a) Isolated star-like object (aster). (b, c) Illustrations of aster and anti-aster magnetic orders. (d) Schematics of the toroidal vortex flows generated by aster in the top and bottom liquids [36]. (e–h) Action of a self-assembled aster-robot. The aster, remotely controlled by an external dc magnetic field applied parallel to the interface, performs simple robotic functions: capture, transport, and release of a large nonmagnetic particle (1-mm glass bead), (movie 4.1). (i–l) A cluster of four asters captures all nonmagnetic beads scattered at the oil/water interface; the particles are trapped in the interstitial space between the asters (movie 4.2); arrows show the direction of the surface flow created by the cluster [36].

For the rather large viscosity of the top liquid (the viscosity of silicone oil is about 20 times higher than the viscosity of water), in addition to magnetic snakes, a new type of dynamically self-assembled patterns is observed: axi-symmetric asters and clusters of asters. The asters are composed of chains with the magnetic moments pointing towards the center (asters) or out of the center (anti-asters) (Fig. 4a–c). While asters are immobile, they create a rectified toroidal vortex flow pointing down in the bottom liquid and up in the top liquid layer (Fig. 4d). Obviously, the magnetic order of asters is highly unfavorable under equilibrium conditions: asters rapidly disintegrate when the applied ac magnetic field is switched off. Application of a small dc magnetic field H_{dc} parallel to the interface between liquids results in controlled self-propulsion of the asters: they open up and swim in the direction of the field, with the asters and anti-asters swimming in opposite directions. It is important to emphasize that a homogeneous dc magnetic field exerts no net force on the aster: the propulsion is an outcome of a distortion of the aster's magnetic structure and consequent deflection of the rectified streaming flow from the vertical direction.

The in-plane component of the rectified flow propels the aster along the field direction. The swimming velocity V initially increases with the increase in in-plane field H_{dc}, reaches a maximum at some value, and finally vanishes for a relatively strong field (about 20 Oe for reported experimental conditions). A simple theoretical prediction based on approximation of an aster by a pair of magnetic spheres gives the following dependence of the aster's speed V on in-plane field H_{dc}:

$$V \sim H_{dc}(H_c^2 - H_{dc}^2)\,. \tag{3}$$

Thus, the shape of the asters and their swimming direction can be remotely controlled by a small in-plane magnetic field.

This functionality enables asters and clusters of asters to perform simple robotic functions: capture, transport, and positioning of target particles [36] (Fig. 4e–h). A cluster of four asters, shown in Fig. 4i–l, exhibits an additional functionality not present in a single aster: the possibility of capturing nonmagnetic particles in the interstitial space between the asters.

In addition to the colloidal assembly at the interface, the patterns can be formed in the bulk. It was shown in [35, 55, 60, 61] that in an alternating field, either electric or magnetic, the dipolar colloidal particles may assemble into planar sheets: a rotating planar field generates $1/r^3$ dipolar pair interaction with in-plane attraction (r being the distance between particles) and repulsion along the rotation axis. This anisotropic interaction forces the particles to assemble into flat sheets parallel to the field plane [60]. In the case of a triaxial field, the interactions are more complicated, and, as was shown in [55, 61], can become, under certain conditions, isotropic. The special case of a precessing triaxial magnetic field was studied in [35]: the field has a cone opening angle θ_m which is controlled by the ratio of the static component (z-component) to the rotating component (x, y components). The field-induced interaction between superparamagnetic particles decays as α/r^3 with the interparticle distance r. The constant α depends on the opening angle θ_m: for small θ_m the colloid behaves like a dipolar liquid. For the opening angle $\theta_m \approx 90^\circ$, the colloidal particles experience effective in-plane attraction [60, 62]. For the so-called 'magic angle',

$$\theta_m = \arctan \frac{1}{\sqrt{3}} \approx 54.7^\circ , \tag{4}$$

the time-averages interaction term vanishes irrespectively of the relative position of the particles. In this case, the interaction becomes isotropic and attractive, and decays as $1/r^6$, somewhat similar to the van der Waals interaction between molecules.

When a triaxial magnetic field with the opening angle close to the magic angle was applied to a suspension of micron-size superparamagnetic particles, a formation of ordered planar membranes consisting of closed-packed particles was observed [35]. The gradual formation of these membranes from a semi-dilute suspension of particles is illustrated in Fig. 5a–e. The particles initially assemble into dimers; the dimers form chains and Y-junctions. The Y-junctions eventually interconnect and coarsen, giving rise to patches of membranes of all orientations. The membranes show a remarkable self-healing capability: a membrane reconstitutes its structure after an artificial perforation is created. In addition to dense membranes, a rich variety of complex patterns was observed in a rotating (vortex) magnetic field: periodic lattices, honeycomb-like 'particle foams' (Fig. 5f–h) [61], sheets of spinning chains [63], various dynamically-assembled clusters, etc. [64]. When both electric and magnetic fields were applied, the reversible assembly/disassembly of magnetic Janus particles into novel staggered chain structures was observed [65].

3. Self-propelled colloidal systems

In this section, we consider colloidal suspensions of self-propelled particles. The interest in such systems is driven by a growing demand for nanotechnological applications based on autonomously moving devices capable of performing useful functions on a microscale. These applications include

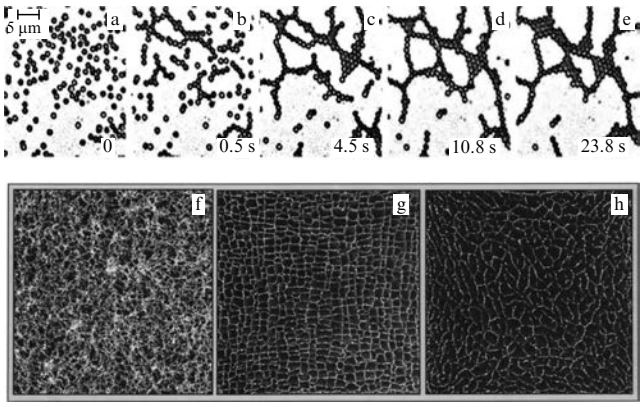

Figure 5. (Color online) (a–e) Formation of a self-healing membrane from a dilute suspension of superparamagnetic particles (0.15 particles per μm^3) after a rotating magnetic field field has been switched on. The appearance of short chains (0.5 s) is followed by their growth, branching, and the formation of a loose network (4.5 s). Most remaining unconnected clusters are rapidly captured, and the network is subsequently coarsened such that the membrane patches grow at the expense of the chainlike sections (10.8 s and 23.8 s). (Reproduced with the kind permission of the authors of [35] and the American Physical Society.) (f–h) Select structures made in triaxial magnetic fields. In a triaxial field, a disordered pattern is formed (particle gel) (f). In a two-dimensional heterodyning (with two different frequencies) field, a honeycomb structure forms (g). Three-dimensional heterodyning of the magnetic field leads to a particle foam (h). 50-μm Ni particles are used, images are 1 cm across. (Reproduced with the kind permission of the authors of [55] and the American Physical Society.)

delivery of drug-laden nanoparticles to specific cellular targets (targeted drug delivery) or massive parallel assembly of microscopic machines by autonomously moving agents. A number of original design concepts of such microscopic swimmers have been developed in recent years, including chemically-propelled swimmers energized by a catalytic chemical reaction, and swimmers harvesting the energy of an electric or magnetic field or ultra-violet light radiation; for a recent review, see [41].

3.1 Practical realizations of self-propelled particles

Figure 6 illustrates several practical realizations of microscopic swimmers. A gold-platinum rod, designed by the Sen and Mallouk group [66, 70], swimming in a solution of hydrogen peroxide is shown in Fig. 6a. A typical swimming speed for the $2-3$-μm rod is on the order of 6–10 μm s^{-1}. The current consensus is that the rod is propelled by the self-induced electrophoretic flow powered by the catalytic decomposition of H_2O_2 at the gold/platinum contact. According to Ref. [70], the swimming speed V can be estimated by equating the propulsion force (due to electrochemical reaction) to the drag force:

$$V \sim \frac{SR^2\gamma}{\eta DL} , \tag{5}$$

where L and R are the length and radius of the rod, η is the dynamic viscosity of water, D is the diffusivity of oxygen, γ is the solution/solid interfacial tension, and S is the oxygen generation rate normalized by the surface area. A detailed theoretical consideration of the electrochemical locomotion of bi-metallic rods can be found in [71].

A polystyrene bead half coated by platinum (Janus particle), propelled by the gradient of osmotic pressure due

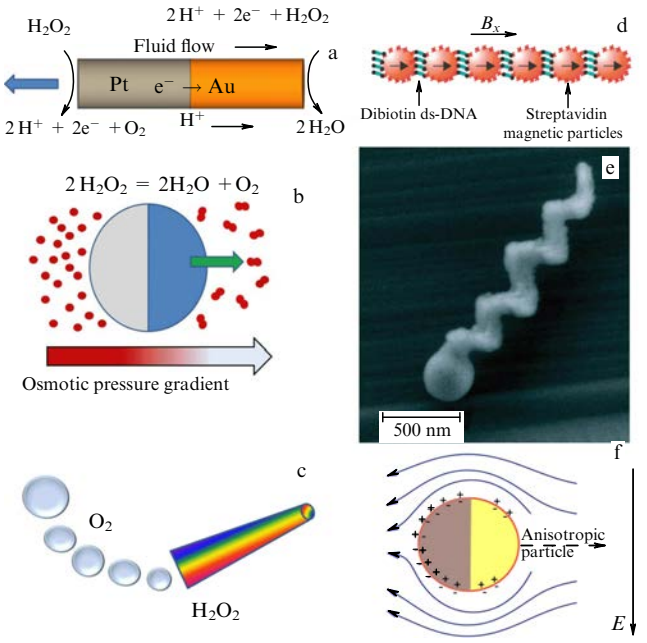

Figure 6. (Color online.) Several practical realizations of microscopic swimmers. (a) A gold-platinum rod propelled by self-electrophoresis in an aqueous solution of H_2O_2 (from [66]). The potential difference created at the Au/Pt contact in the course of catalytic decomposition of H_2O_2 causes electrophoretic flows propelling the rod. Blue arrow depicts swimming direction. (b) Two-sided (Janus) particle propelled by self-diffusiophoresis in an H_2O_2 solution, from [67]. Particles are 1.62-μm polystyrene spheres with one side coated with platinum. (c) High-speed bilayer polyaniline/platinum microtubes (rockets) grown in the conically shaped pores of a polycarbonate template membrane and propelled by O_2 microbubbles in an H_2O_2 solution [68]. (d) Artificial magnetic microswimmer. Superparamagnetic particles are coated with streptavidin (red cross symbols). Under an applied magnetic field B_x, the particles form chains along the field direction. Double-stranded DNA with biotin at each end binds the particles together (biotin and streptavidin are complementary proteins forming strong links). The chain is then attached to a red blood cell and energized by an ac magnetic field perpendicular to B_x (from [31]). (Reproduced with the kind permission of the Nature Publishing Group.) (e) Scanning electron microscopy image of an individual glass screw (nano-propeller) with nano-structured helicity. A 30-nm layer of a ferromagnetic material (cobalt) is deposited on one half of the helix. The propeller is then energized by a rotating triaxial magnetic field [69]. (Reproduced with the kind permission of the American Chemical Society.) (f) A metal–dielectric particle (a 4-μm polystyrene bead partly covered with gold) is propelled by ac electric field. The electric double layer on the gold side (black hemisphere) is more strongly polarized and thus drives a stronger induced charge electroosmosis slip (arrows) than the polystyrene side, resulting in induced charge electrophoresis motion in the direction of the dielectric side [43].

to self-diffusiophoresis, is shown in Fig. 6b. Platinum catalyzes the reduction of hydrogen peroxide (fuel) to oxygen and water, producing more molecules of reaction product than consumed fuel. The characteristic swimming speed is about 2–3 μm s^{-1} [67]. The propulsion velocity V can be estimated by using the lateral gradient of the excess solute concentration in the vicinity of the particle, resulting in

$$V \sim \frac{k_B T l^2 k}{\eta D}, \tag{6}$$

where k is the reaction rate, k_B is the Boltzmann constant, T is the temperature, and l is the range of of the interaction zone between the particles and the solute. While the details of the propulsion kinetics for bi-metallic rods and Janus particles are different (electrophoresis vs diffusionphoresis), the expressions for swimming speeds, Eqns (5) and (6), are similar.

A high speed microtube conical rocket developed by J Wang's group, UCSD, is shown in Fig. 6c. The rocket is propelled by O_2 bubbles in a hydrogen peroxide solution and swims up to 350 body lengths per second; typical rocket size is 5–10 μm [68]. Similar bubble-propelled particles (nanosubmarines) have also been designed by O Schmidt's group [72]. In contrast to Janus particles and gold-platinum rods, the decomposition of the hydrogen peroxide occurs on the inner Pt surface of the conical rocket, and thus does not have the ionic-strength limitation of catalytic bi-metallic rods.

In addition to chemical reactions, self-propelled colloidal particles can be energized by ac electric or magnetic fields. Some of these design concepts are inspired by Nature. Figure 6d shows artificial microswimmers (magnetic sperm) [31]. The swimmer is assembled from a dilute suspension of superparamagnetic nanoparticles linked by DNA molecules and attached to a red blood cell (cargo). The direction of swimming is prescribed by an applied dc magnetic field B_x, which orients the magnetic chain (flagellum). The swimmer is then energized by an ac magnetic field B_{ac} applied perpendicular to B_x. The typical size of the swimmer is about 5 μm, and the speed is about 20 μm s^{-1}, similar to that of motile bacteria. For this kind of artificial swimmer, the relevant dimensionless parameter characterizing the propulsion ability is the so-called sperm number S_p:

$$S_p = L\left(\frac{\xi_\perp \omega}{\kappa}\right)^{1/4}, \tag{7}$$

where L is the length of the filament, κ is its bending rigidity, $\omega = 2\pi f$, f is the frequency of the ac magnetic field B_{ac}, and $\xi_\perp$ is the perpendicular viscous friction coefficient.[3] The sperm number represents the relevance of viscous to elastic stresses on the filament. The experiments revealed that maximum dimensionless propulsion speed $V/L\omega$ occurs for $S_p \approx 3$ [31].

Another design of a microswimmer, inspired by a bacterium propelled by the rotation of helical flagella, is presented in Fig. 6e. A half of a nanoscale glass propeller is covered by ferromagnetic material (cobalt) and brought into motion by a rotating magnetic field [69]. These cork-screw particles can swim up to 40 μ s^{-1}. A magnetic swimmer based on a rotation of a magnetic doublet coupled to a boundary interaction was studied in Ref. [32]. In the broader context of magnetic swimmers, the self-assembled snake [33], discussed in the previous section, is different from all of these designs, since it utilizes self-propulsion due to a spontaneous symmetry breaking.

Metal-dielectric microparticles can be brought into motion by an ac electric field [43, 74]. In this case, the particles move perpendicular to the field direction by induced-charge electrophoresis, arising due to 'induced-charge electroosmosis', i.e., the action of an applied electric field on its own induced diffuse charge near a polarizable surface. For typical experimental conditions, the speed of particles perpendicular to the applied field was on the order of 30 μm s^{-1} (Fig. 6f). This phenomenon may find applications in various microfluidic devices.

[3] The hydrodynamic slender body theory gives for long thin filaments $\xi_\parallel/\xi_\perp \approx 2$, where $\xi_\parallel$ is the tangential friction coefficient [73].

3.2 Individual and collective motion of colloidal microswimmers

Figure 7 shows trajectories of individual self-propelled gold/platinum rods and platinum–silica Janus particles. The trajectories are not straight lines; the orientation of the particles changes randomly, likely due to thermal diffusion and interaction with gas microbubbles created earlier by other particles. Additional factors contributing to the diffusive-like behavior are imperfections of the rods, like roughness of the surface, curvature etc. The overall behavior is similar to the so-called run-and-tumble motion of motile bacteria [75]. In this context, one can discuss mean-square displacement (msd) of the colloidal particle, Δr^2. According to the Stokes–Einstein relation for a Brownian particle of radius R, the msd is linear in time, $\Delta r^2 \sim 6Dt$ in three dimensions and $\Delta r^2 \sim 4Dt$ in two dimensions, where $D = k_B T/(6\pi\eta R)$ is the particle's diffusion coefficient.[4] The particle will also perform rotational diffusion with the characteristic time scale τ_r. For a self-propelled particle moving with the velocity V, the direction of motion itself will be subject to rotational diffusion, leading to coupling between the translational and rotational motions. In this case, the self-propulsion results in a significant increase in the effective diffusion coefficient. According to [67], the two-dimensional projection of the msd is of the form[5]

$$\Delta r^2 = 4D\Delta t + \frac{V^2\tau_r^2}{2}\left[\frac{2\Delta t}{\tau_r} + \exp\left(-\frac{2\Delta t}{\tau_r}\right) - 1\right], \qquad (8)$$

where Δt is the observation time. For short times, $\Delta t \ll \tau_r$, the motion of the particles is roughly ballistic, $\Delta r^2 \approx 4D\Delta t + V^2\Delta t^2$. For long times, $\Delta t \gg \tau_r$, we obtain from Eqn (8)

$$\Delta r^2 \approx 4D\Delta t + V^2\tau_r\Delta t = 4D_{\text{eff}}\Delta t\,. \qquad (9)$$

Thus, due to the coupling between translation and rotation, the particle performs random walk with the effective diffusion coefficient $D_{\text{eff}} = D + V^2\tau_r/4$. Self-propulsion can, therefore, result in a significant increase in a particle's self-diffusion.

One of the fundamental issues in the context of artificial microswimmers is the possibility of collective motion for higher concentrations, similar to that exhibited by swimming bacteria, where large-scale patterns of collective locomotion, arising purely from collisions and hydrodynamic interactions, have been observed [76, 77] (see Fig. 10a in Section 4.2). Collective motion of microswimmers has many advantages compared to individual swimming, for example, from the perspective of collective cargo delivery or harvesting the mechanical energy of chaotic motion [78]. To date, no collective behavior similar to that of bacterial systems has been observed in the concentrated suspensions of artificial swimmers. The main reason is possibly due to a too high rotational diffusion of individual particles, which destroys the collective swimming state. In addition, gold/platinum particles show a tendency to form aggregates after a collision. Experiments [79] and simulations [80] with dense suspensions of self-propelled Janus colloids showed the merging and breaking of transient aggregates of particles; the average size of the aggregates grows linearly with the self-propelling velocity.

[4] Here we used the expression for viscous drag force F_d acting on a spherical particle: $F_d = 6\pi\eta RV$ [59].

[5] Systematic particle tracking for the majority of colloidal systems is possible only in two dimensions.

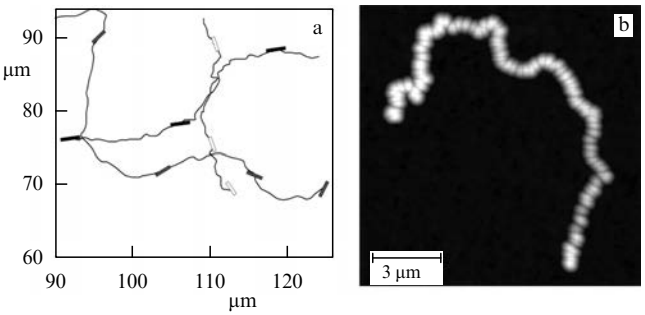

Figure 7. Trajectories of self-propelled particles. (a) Representative trajectories of several individual gold/platinum rods in H_2O_2 solutions, from [70]. (Reproduced with the kind permission of the American Chemical Society.) Intervals of ballistic motion are interrupted by sharp turns, similar to the run-and-tumble behavior of motile bacteria. (b) Projection of 120 frames of a 1-μm half-coated Pt-silica particle traveling in a 10% w/w H_2O_2 solution [81]. (Reproduced with the kind permission of the American Chemical Society.)

A variety of collective chemical responses of artificial swimmers to ultraviolet (UV) light irradiation was reported in Refs [82–84]. Upon ultraviolet light illumination, it was observed that 1 μm silver on silica Janus particles migrate away from the irradiated regions [83]. This behavior is reminiscent of a phototactic response (a tendency to navigate towards light) of biological systems, shown, for example, by some green algae. An interesting 'schooling' behavior was exhibited by micron-size silver chloride (AgCl) particles upon UV irradiation [82]. AgCl particles move autonomously in deionized water by self-diffusiophoresis due to asymmetric AgCl decomposition under the UV light. A moving AgCl particle releases ions, to which the other particles respond by drifting or 'schooling' into regions with higher particle concentrations. When photo-inactive silica particles are mixed with the AgCl, they respond to the ion release by swimming towards and surrounding individual AgCl particles (Fig. 8). Collective chemical oscillations were also observed in a suspension of AgCl particles in the presence of

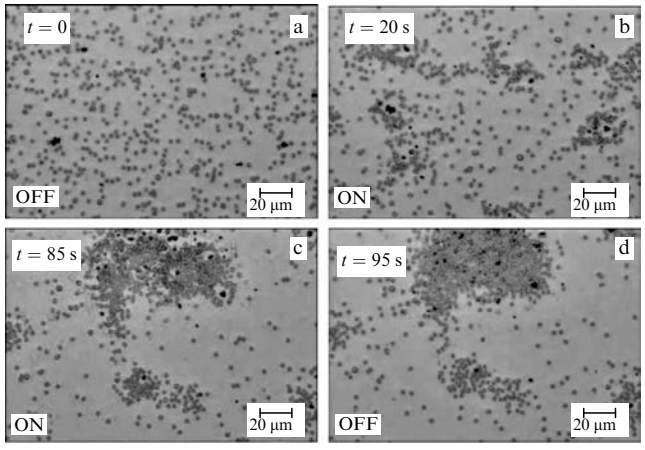

Figure 8. 'Predator–prey' behavior shown by 1-μm AgCl particles (darker objects) and 2.34-μm silica spheres mixed in deionized water. When irradiated with ultraviolet (UV) light (a–c), the silica spheres actively seek out the AgCl particles and surround them. A 2–3-μm exclusion zone is seen around the AgCl particles while the UV light is on; it disappears when the UV light is turned off (d) [82]. (Reproduced with the kind permission of John Wiley and Sons.)

UV light in a dilute hydrogen peroxide solution [84]. Both single-particle and collective, multi-particle responses were observed due to an oscillatory, reversible conversion of AgCl to silver metal on the particle surface. The collective motions of these light-powered microswimmers self-organize into clumped (clustered) chemical oscillators with significant spatiotemporal correlations between the particles.

4. Biocolloids: suspensions of swimming microorganisms

While there are obvious differences between the suspensions of living bacteria and inanimate colloidal systems, there are also many similarities, especially with the systems of artificial swimmers considered in Section 3. For example, the size of the common aerobic rod-shaped bacterium *Bacillus subtilis* is about 5 μm, and typical swimming speed is on the order of 20 μm s^{-1}, similar to that of many artificial swimmers. As a result, in addition to 'pure biological mechanisms', like chemotaxis, cell division etc., the bacteria experience the same spectrum of forces as colloidal self-propelled particles of a similar size: hydrodynamic entrainment, steric repulsion, buoyancy, and thermal fluctuations. Since the Reynolds number for an individual bacterium is exceedingly small, the effects of fluid inertia can be neglected.[6] In addition, some bacteria may possess a permanent magnetic moment (so-called magnetotactic bacteria like *Magnetospirillium magnetotacticum*), and, therefore, they can be manipulated and assembled by an external magnetic field [85, 86].

4.1 Collective behavior

Motile (swimming) microorganisms, like many bacteria, propel themselves in viscous fluid by a rotation of flagella and often develop large-scale patterns of collective locomotion with a characteristic length scale significantly exceeding the size of a single microorganism (see Section 4.2, Fig. 10a). The collective behavior of motile aerobic bacteria, especially at high concentrations, is governed by a subtle interplay among buoyancy, hydrodynamic interactions, oxygen consumption, and collisions. The recent consensus is that the collective motion and self-organization in the suspensions of swimming bacteria often arise due to pure 'physical mechanisms': hydrodynamic interactions between the organisms and short-range collisions (Fig. 9), whereas specific biological mechanisms, such as chemotaxis [75], play a relatively minor role. Large-scale self-organization is driven by the input of mechanical energy from the rotating bacterial flagella. Thus, in contrast to high Reynolds number hydrodynamic turbulence, the energy injection in bacterial suspensions occurs on a microscopic scale.

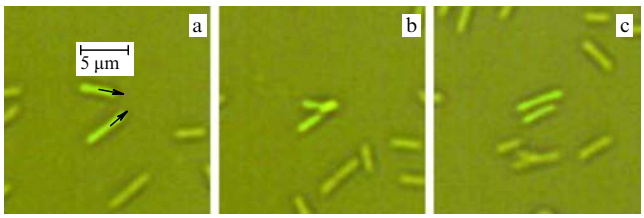

Figure 9. (Color online.) A sequence of images illustrating a collision event between two swimming bacteria *Bacillus subtilis* in a thin free-standing liquid film [77]. Black arrows indicate the swimming direction. The collision results in an alignment of bacteria.

[6] For a bacterium of length $L = 5$ μm swimming with the speed $V = 20$ μm s^{-1} in water, and kinematic viscosity of water $\nu = 0.01$ cm^2 s^{-1}, the corresponding Reynolds number is $\mathrm{Re} = LV/\nu \approx 10^{-4}$.

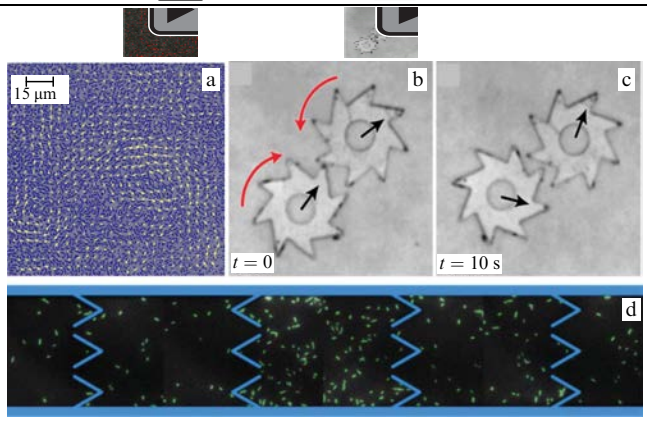

Figure 10. (Color and animation online.) (a) Collective motion in a concentrated suspension of motile bacteria *Bacillus subtilis*; bacteria are seen as short dark stripes, arrows indicate the direction of bacterial flow [77]. The collective swimming is manifested by a formation of swirls and jets with the characteristic scale exceeding the length of a bacterium by an order of magnitude (movie 10.1 courtesy of Andrey Sokolov). (b, c) Motile bacteria *Bacillus subtilis* power microscopic (0.5 mm) gears; each gear is about one million times heavier than an individual bacterium (movies 10.2 and 10.3) [78]. (d) Fluorescence micrograph of individual motile bacteria *Escherichia coli* (labeled green) inside a microchannel with funnel-shaped barriers. The chambers, where the rectification bias is reversed, have a higher concentration of bacteria [88].

Experimental studies of suspensions of *Bacillus subtilis* revealed that at a concentration above some critical one, a gradual transition from random swimming to collective locomotion occurs [76, 77]. The collective motion is characterized by a sixfold to eightfold increase in the velocity correlation length and up to a sixfold increase in the swimming speed of bacteria. Such a dramatic increase in the swimming speed in the collective motion mode is likely an outcome of two effects: hydrodynamic drag reduction in more dense bacterial 'packs' and more efficient energy injection due to synchronization of bacterial flagella by hydrodynamic coupling [87].

4.2 Rectification of random motion

Suspensions of swimming bacteria exhibit material properties very different from suspensions of passive particles. It was found recently that in concentrated suspensions of motile bacteria, such as *Bacillus subtilis*, *Escherichia coli*, the activity (i.e., swimming) results in a reduction of viscosity [44] and a dramatic increase in diffusivity [45, 46, 89]. Moreover, it was demonstrated that it is possible to harvest the mechanical energy of random bacterial motion [78]. While the laws of thermodynamics prohibit extraction of useful work from the Brownian motion of particles in equilibrium, these motions can be 'rectified' under nonequilibrium conditions, for example, in the presence of asymmetric geometrical obstacles. This is demonstrated by Fig. 10b, c, where aerobic bacteria *Bacillus subtilis* moving randomly in a suspended fluid film power submillimeter gears decorated with asymmetric teeth and an assembly of gears. The gears' angular velocities can be controlled by the amount of oxygen available to the bacteria. In contrast to passive particles, the bacteria slide along the slanted edges of the gear's teeth and become trapped in the corners at the tooth junctions for extended

periods of time before finally escaping these 'traps'. Since bacteria are self-propelled objects, they push against the gear wall during the trapping events and effectively transfer momentum to the gear.

Let us consider here how much power W_g a gear can extract from the chaotic motion of bacteria. This power can be estimated as $W_g \sim f_r \Omega^2$, where f_r is the rotational drag coefficient, and Ω is the gear's rotation rate. Approximating a gear by a thin disk of radius R, one obtains $f_r \approx 32\eta R^3/3$ [73]. For typical experimental conditions, $R \approx 200$ μm, and $\Omega \approx 1/10$ rad s^{-1} (1 rotation per minute), giving $W_g \sim 10^{-16}-10^{-15}$ W, i.e., on the order of a few femtowatts. A single bacterium delivers power on the order of $W_b \sim f_b V^2 \sim 10^{-18}-10^{-17}$ W, where f_b is the translational viscous drag coefficient for a single bacterium. Thus, only a few hundred bacteria are needed to rotate one microgear.[7] The ability to harness and control the power of collective motions appears to be an important requirement for further development of mechanical systems driven by microorganisms or synthetic swimmers.

Figure 10d illustrates rectification of bacteria concentration in microfluidic chambers with ratchet funnel walls [88]. In equilibrium, the averaged concentration of bacteria should be identical in all chambers. However, since the bacterial suspension is a nonequilibrium system, it is possible to trap most of the bacteria in one chamber due to a rectification bias imposed by the ratchet walls. The mechanism of rectification is similar to that described above.

4.3 Reduction of viscosity

The way in which swimming microorganisms alter the effective properties of the suspension depends on the type of propulsion. For example, most swimming bacteria are propelled from behind, by the rotation of helical flagella. In contrast, unicellular algae like *Chlamydomonas reinhardtii* swim by beating two cilia protruding forward from the body. As a result, the flow patterns created in the course of swimming by these microorganisms are very different. Since no net force is applied to a self-propelled particle, the microorganism imposes a *force dipole* on a suspending fluid — the propulsion force is compensated by viscous drag. Far from the microorganism, the hydrodynamic flow velocity $\mathbf{v}$ is therefore described by a point hydrodynamic dipole:

$$\mathbf{v} = -u_0 \mathbf{r}\left(\frac{3(\mathbf{rd})^3}{r^5} - \frac{1}{r^3}\right), \qquad (10)$$

where $\mathbf{d}$ is the unit vector of dipole orientation, $\mathbf{r}$ is the radius vector relative to the center of the dipole, and $u_0 = \alpha V_0 L^2$ is the hydrodynamic dipole strength [73] (V_0 is the magnitude of swimming speed, L is the length of a bacterium, and $\alpha \sim 0.1-0.3$ is a factor determined by the shape of a bacterium). The sign of the dipole u_0, however, depends on the details of propulsion, and is negative for bacteria-like swimmers (pushers) and positive for algae-like swimmers (pullers). The asymptotic flow field of a bacterium is shown in Fig. 11a. The corresponding flow fields of swimming bacteria [90] and unicellular algae [91] were measured directly.

To understand the effect of bacteria on suspension's rheological properties, consider the following simple arguments [92]. Since the bacterium has a rod-like cell body (aspect ratio is about 5), it will be oriented by a shear flow. For example, in a pure shear flow, the bacterium will align along the stable axis of the flow (Fig. 11b). Since the bacterium is a force dipole, it does not create an extra force on any external wall, and, therefore, does not change the measured shear stress. However, it will accelerate the liquid along the swimming direction, thus increasing the shear strain rate of the flow. As a result, the effective viscosity, being a ratio of shear stress to strain rate, will decrease in the presence of bacteria. In contrast, the algae-type swimmers (pullers) will increase the viscosity of the suspension.

Experimental studies on the suspensions of various microorganisms have indeed revealed a significant decrease in viscosity for the suspensions of bacteria [44] and an increase in viscosity for the suspensions of algae [93]. The dependence of viscosity on the concentration of bacteria n is shown in Fig. 12. A sevenfold decrease is observed for relatively high concentrations, in the collective motion mode. With a further

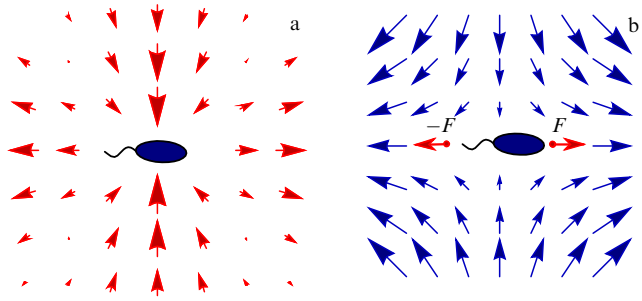

Figure 11. (Color online.) (a) Fluid velocity field created by a swimming bacterium; the swimming dipole creates a flow velocity field with a quadrupolar symmetry [73]. (b) Pure shear (elongational) flow orients a bacterium along the stable direction. The bacterium creates a force dipole with the magnitude F (indicated by red arrows) and accelerates the flow, resulting in a reduction of the effective viscosity.

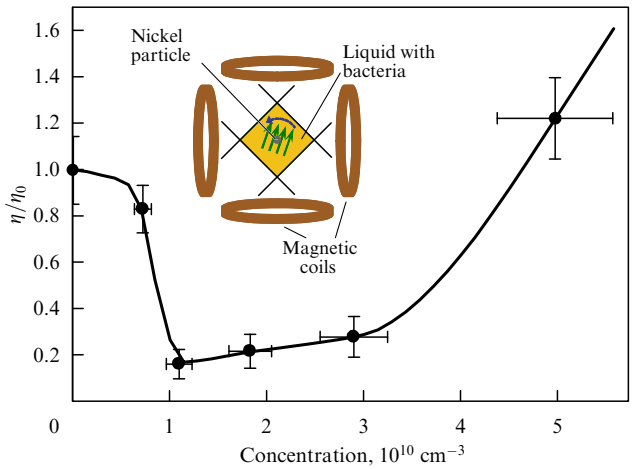

Figure 12. Illustration of viscosity reduction in suspensions of motile bacteria *Bacillus subtilis* [44]. With an increase in bacterial concentration, the effective viscosity of suspension η decreases up to sevenfold compared to the viscosity of suspending liquid η_0. Inset shows the schematics of the experimental setup. A magnetic (nickel) particle is immersed in a free standing liquid film containing bacteria *Bacillus subtilis*. The particle is spun by a rotating magnetic field created by a set of coils; the viscosity is extracted from the measurement of magnetic torque exerted on the particle.

[7] Here we used for the bacterial swimming speed $V \approx 20$ μm s^{-1}, effective bacterium size $a = 2-5$ μm, and translational viscous drag coefficient $f_b = 6\pi\eta a$.

increase in the concentration of bacteria, the viscosity increases again; the upturn is likely due to a jamming of the cells, slowdown of metabolism, an accumulation of waste products, etc.

While the experimental results qualitatively comply with the trend predicted by simple arguments [92], in reality the situation is far more complex. In particular, the experiments are performed in the geometry close to a planar shear flow (flow between two parallel moving walls) rather than pure shear (elongational) flow. In this case, the individual bacterium will be rotated by the flow, instead of aligning along the stable axis [73]. It was shown in theoretical studies that, in addition to the energy injection by swimming bacteria, in the case of planar shear flow one needs to take into account hydrodynamic interactions between the swimmers and their random reorientations (tumbling) in order to explain the reduction of viscosity [94, 95].

5. Theoretical approaches

Since active colloids are out of thermal equilibrium, the powerful machinery of thermodynamics and statistical physics developed for equilibrium systems, e.g., various techniques based on minimization of energy or maximization of entropy, can not be applied in the majority of cases. Thus, direct numerical modeling of colloidal suspensions and simplified phenomenological models have become the most popular research tools. Here, we present a very short (and far from complete) overview of some theoretical and computational approaches.

Different theoretical approaches are often applied to the same experimental system. Continuum coarse-grained models, derived for macroscopic degrees of freedom (concentrations, velocities, polarization, etc.), are more computationally effective than direct particle simulations, and, in general, provide better insights: they depend on a significantly smaller number of parameters, and allow studying bigger systems on longer times scales. On the flip side, systematic derivation of the coarse-grained equations in the out-of-equilibrium situation is a formidable challenge.

5.1 Discrete particle simulations

Figure 13 illustrates the comparison between the results of computer modeling and experiments in suspensions energized by electric [96] or magnetic fields [55] (see Figs 1 and 5). In most cases, there is good qualitative — and sometimes even quantitative — agreement between experiment and computer simulations. While the systems under study are rather different (charged particles in [18, 47] and magnetic particles in [55]), the simulation approaches, different in the details of implementation, have some similarities. In both cases the time evolution of the individual colloidal particle is governed by an overdamped Langevin equation with thermal noise (Brownian dynamics). Colloidal particles are typically treated as hard spheres or discs, with either a fixed dipole moment [55] or electric charge [96], while the hydrodynamic interactions between particles are neglected. Since the implementation of collisions between hard disks or spheres is associated with significant computationally challenges (see, e.g., [97]), 'softened' hard core potential is often used instead: the Lennard-Jones potential or the stiffer repulsive potential

$$V(r_{ij}) = \frac{V_0 \exp\left[-(r_{ij}-a)/\lambda\right]}{r_{ij}-a}\,,$$

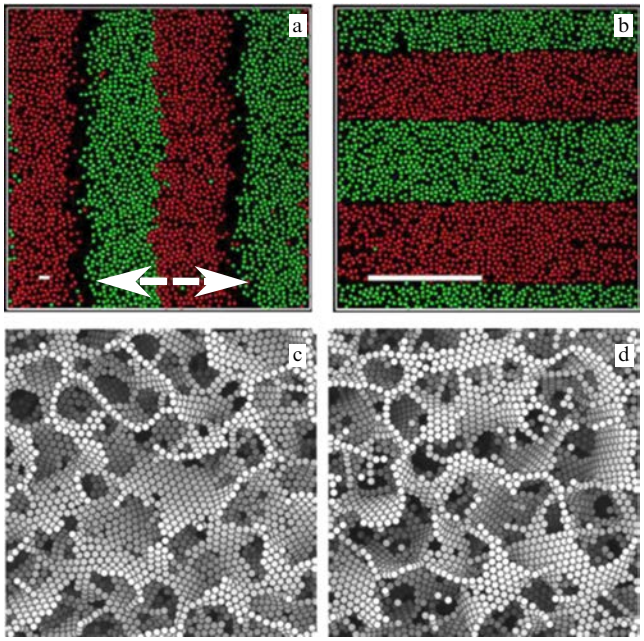

Figure 13. (Color online.) (a, b) Brownian dynamics simulations of a mixture of two oppositely charged colloids; direction of the driving ac electric field is indicated by the broken white arrow, the solid bar size is proportional to the driving force, i.e., field amplitude. In agreement with the experiment [18, 47] (see Fig. 1e, f), static bands are formed perpendicular to the field direction for small driving forces, and lanes are formed parallel to the field's direction for higher driving forces [96]. (c, d) Computer modeling of structures produced in a suspension of magnetic colloids by the ac tri-axial magnetic field. Image (c), produced by the three-dimensional heterodyning fields, is indistinguishable from the image (d), generated by simulated annealing (due to thermal fluctuations, no field; compare to Fig. 5h) [55]. (Reproduced with the kind permission of the American Physical Society.)

where $r_{ij} = |\mathbf{r}_i - \mathbf{r}_j| > a$ is the distance between particles, a is the particle radius, and V_0 and λ are the potential strength and decay length.

The Brownian dynamics can be illustrated for the system of two oppositely charged colloids energized by an electric field [96]. Particles of sorts A and B are subject to oscillatory force $\mathbf{f}^{\mathrm{A}}(t) = -\mathbf{f}^{\mathrm{B}}(t) = f_0 \sin(\omega t)\mathbf{e}_x$, where f_0 and ω are the magnitude and frequency of the driving field, respectively. Equations of motion have the form

$$\zeta^{\mathrm{A,B}}\dot{\mathbf{r}}_i^{\mathrm{A,B}} = \mathbf{f}^{\mathrm{A,B}} - \sum_{i\neq j}\frac{\mathrm{d}V(r_{ij})}{\mathrm{d}r_j} + \xi_i(t)\,, \qquad (11)$$

where $\zeta^{\mathrm{A,B}}$ are the particles' mobilities, $\mathbf{r}_i^{\mathrm{A,B}}$ are the positions, and ξ is a random force (thermal noise). Despite these drastic simplifications, the simulations often reproduce key experimental observations: the formation of lanes [96] and 'colloidal foams' [55]. It was shown in [98] that the hydrodynamic interactions between the particles, while critical in some cases, appear to be unimportant for strongly driven oppositely charged colloids, i.e., for lanes.

5.2 Continuum models

The theoretical description becomes significantly more challenging when the flows generated by colloidal particles are crucial, i.e., in the case of pulsating rings and rotating vortices studied in [48] and self-assembled magnetic swimmers [33]. The phenomenological continuum model based

on coupled equations for the evolution of particle concentration and self-induced electro-osmotic flows was proposed in Ref. [52]. The model operates in terms of two-dimensional concentrations (averaged over the vertical coordinate z) of two types of particles: the concentration of gas, i.e., rapidly moving particles ρ_g, and the concentration of immobile particles, or precipitate ρ_p. While the separation into gas and precipitate is somewhat artificial, it allows us to reduce the computational complexity of the problem. Since the total number of particles N is conserved, $N = \int(\rho_p + \rho_g)\,dx\,dy = \text{const}$, the dynamics is described by the corresponding conservation laws

$$\partial_t \rho_g = -\nabla \mathbf{J}_g + \tilde{f}, \qquad \partial_t \rho_p = \nabla \mathbf{J}_p - \tilde{f}, \tag{12}$$

where $\mathbf{J}_{g,p}$ are the corresponding mass fluxes, and function $\tilde{f}$ describes the gas/precipitate conversion which depends on $\rho_{g,p}$, the applied vertical electric field E, and conductivity of the electrolyte (proportional to the concentration of alcohol c). The fluxes can be written in the following generic form (a combination of diffusive and advective fluxes)

$$\mathbf{J}_{g,p} = -D_{g,p}\nabla\rho_{g,p} - \alpha_{g,p}(E)\,\rho_{g,p}\mathbf{v}_\perp\left(1 - \beta_{g,p}(E)\,\rho_{g,p}\right). \tag{13}$$

Here, $D_{g,p}$ are the diffusivities, and $\alpha_{g,p}$, $\beta_{g,p}$ are linear/quadratic advection coefficients for each fraction. The term $1 - \beta_{g,p}\rho_{g,p}$ describes flux saturation for large particle concentrations. $\mathbf{v}_\perp$ is the horizontal (in-plane) velocity of the liquid. The horizontal velocity $\mathbf{v}_\perp$ can be obtained from the incompressibility condition $\nabla\mathbf{v}_\perp + \partial_z v_z = 0$. Assuming that the vertical vorticity $\omega_z = \partial_y v_x - \partial_x v_y$ is small compared to the in-plane vorticity, for $\omega_z = 0$ the horizontal velocity can be obtained from the quasipotential ϕ: $\mathbf{v}_\perp = -\nabla\phi$. The incompressibility condition then yields

$$\nabla^2\phi = \partial_z v_z\,. \tag{14}$$

In turn, the depth-averaged vertical (z) component of velocity $V = h^{-1}\int_0^h v_z\,dz$, where h is the thickness of the cell, can be obtained from the corresponding Navier–Stokes equation (see for detail [52]):

$$\partial_t V = \nu\nabla^2 V - \zeta V + cE\int K(|\mathbf{r} - \mathbf{r}'|)(\rho_g + \rho_p)\,d\mathbf{r}'\,, \tag{15}$$

where ν is the kinematic viscosity, ζ accounts for the dissipation due to friction with the walls, and the last term describes the depth-averaged force acting on charged weakly conducting fluid containing charged microparticles. $K(|\mathbf{r} - \mathbf{r}'|)$ is a phenomenological localized kernel which determines the scale of emergent patterns. With the appropriate choice of the model parameters and functional form of the conversion rate $\tilde{f}$, the model captured, on a qualitative level, the entire complexity of the experimental phase diagram, as well as the primary patterns observed in the experiment: static crystals, honeycomb lattices, and even dynamic pulsating rings and rotating vortices (Fig. 14a–f).

A hybrid model based on discrete particle dynamics and a continuum hydrodynamic model for the liquid was used to describe the formation of self-assembled magnetic snakes and swimmers [58] (Fig. 14g–i). In this approach, the Newton equations for positions and orientations of colloidal particles at the interface between air and water were coupled to the Navier–Stokes equation for the fluid flow. The full nonlinear Navier–Stokes equation (rather than the linear Stokes equation) is necessary for describing the rectified large-scales flows generated by the snakes. To reduce the computational load associated with the numerical solution of the three-dimensional nonlinear partial differential equation for the fluid flow, the Navier–Stokes equation was solved in a much simpler shallow water approximation [59] for the depth-averaged horizontal velocity $\mathbf{v}$, valid when the thickness of water layer h becomes small compared to the size of a magnetic snake. These equations are of the form

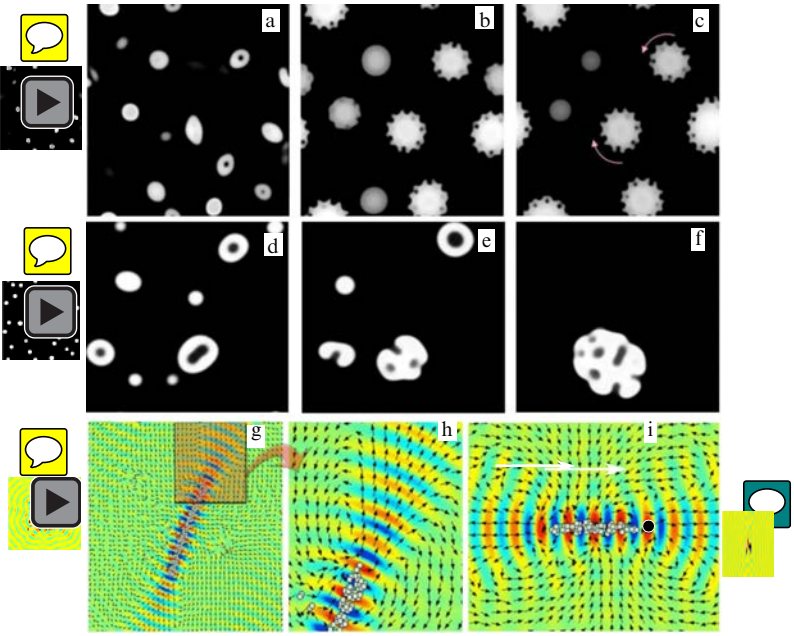

Figure 14. (Color and animation online.) (a–c) Formation of rotating vortex 'stars' in the model of electrostatically driven nonaqueous suspension of conducting microparticles, (movie 14.1) [52]. (d–f) Rotating vortices transform into randomly pulsating rings upon reversal of the direction of an applied electric field (movie 14.2). The structures obtained by computer modeling qualitatively resemble those observed experimentally; compare Fig. 2a–c, rotating stars and (d–i), pulsating rings. (g) Magnetic snake formed from 225 initially randomly distributed particles at the water–air interface; colors indicate elevation of the water surface, and arrows denote hydrodynamic surface flow generated by the snake (movie 14.3). (From [58].) (h) Flow pattern in the vicinity of the snake's tail. (i) Self-assembled swimmer formed by a snake attached to a nonmagnetic bead (large black circle); white arrow indicates the direction of swimming (movie 14.4); compare to images shown in Fig. 3b–f.

$$\partial_t h + \nabla h\mathbf{v} = 0\,, \tag{16}$$

$$\partial_t\mathbf{v} + \mathbf{v}\nabla\mathbf{v} = \nu(\nabla^2\mathbf{v} - \zeta\mathbf{v}) - \nabla h + \sigma\nabla\nabla^2 h + H_0\sin(\omega t)\sum_j s(\mathbf{r} - \mathbf{r}_j)\mathbf{p}_j\,. \tag{17}$$

Here, σ is the surface tension, and ζ describes friction with the bottom. The last term describes the flow generated by the vertical ac magnetic field with the magnitude H_0 and frequency ω acting on magnetic dipoles with the orientation $\mathbf{p}_j = (\cos(\phi_j), \sin(\phi_j))$, and function $s(r)$ describes the particle's shape. The positions $\mathbf{r}_j$ and orientations ϕ_j of the particles are governed by the following Newton equations of motion:

$$m_p\ddot{\mathbf{r}}_j + \mu_t\dot{\mathbf{r}}_j = \mathbf{F}_j + \mu_t\mathbf{v} - \beta\nabla h\,, \tag{18}$$

$$I_p\ddot{\phi}_j + \mu_r\dot{\phi}_j = T_j + \Sigma_j + \kappa H_0\sin(\omega t)\nabla h\times\mathbf{p}_j\,, \tag{19}$$

where m_p, I_p, μ_t, and μ_r are the particle's mass, moment of inertia, and translational and rotational viscous drag coefficients, and $\mathbf{F}_j$ and T_j are forces and torques due to magnetic dipole-dipole interaction and steric repulsion between the particles (torques have only one nonzero component). Σ_j is the torque exerted by shear hydrodynamic flow on a solid particle.[8] Equations (17)-(19) have the following meaning: in addition to magnetic and hydrodynamic forces and torques $\mathbf{F}_j$, T_j, and Σ_j, the particles are subject to advection by the hydrodynamic flow ($\sim \mathbf{v}$), sliding down the gradient of the surface due to gravity ($\beta\nabla h$). The last term in Eqn (19) deserves special attention: it describes the magnetic alignment of particles along the direction of projection of the external ac magnetic field parallel to the surface of the fluid. The in-plane component of the field, oscillating with the same frequency ω, appears due to the deformation of the surface, and is proportional to the slope ∇h. This in-plane field facilitates antiferromagnetic ordering of the neighboring segments and is crucial for the formation of snakes and asters. The model Eqns (16)-(19) successfully reproduced the assembly of a snake from random dispersion of the particles, as well as formation of the self-propelled snake-bead hybrid (Fig. 14g–i).

5.3 Kinetic approach

Significant progress has been achieved in the understanding of collective motion in suspensions of self-propelled swimmers via analysis of simplified probabilistic models, while the detailed role of the specific physical mechanism is a matter of active discussion. The most recent theoretical approaches are based on the mean-field Fokker–Plank–Smoluchowski-type kinetic equations for the time-dependent probability density $P(\mathbf{r}, \mathbf{d}, t)$ of finding a particle in a certain position $\mathbf{r}$ with an orientation $\mathbf{d}$. In the majority of these approaches, the hydrodynamic interactions are described in the dilute limit, when the flow field generated by many bacteria is close to a superposition of individual fields [99, 100]. The bacterial collisions are often incorporated via binary collision integral [101]. In the most general form, the kinetic equation can be written as follows:

$$\partial_t P = -\nabla_r\big((V_0\mathbf{d} + \mathbf{u})P\big) - \nabla_n(\omega P) + I_c + D_t\nabla_r^2 P + D_r\nabla_d^2 P\,, \tag{20}$$

where, V_0 is the speed of an individual bacterium with respect to the liquid in the direction of its unit orientation vector $\mathbf{d}$, $\mathbf{u}$ is the hydrodynamic velocity induced by all swimming particles, $\omega = (\mathbf{I} - \mathbf{dd})(\gamma\mathbf{E} + \mathbf{W})\mathbf{d}$ is the rotational velocity induced by bacteria, $\mathbf{E}$ and $\mathbf{W}$ are the rate of strain and vorticity tensors, γ is the shape parameter which is close to one for slender bodies like bacteria, D_t and D_r are translational and rotational diffusions (e.g., due to tumbling), and ∇_r and ∇_d are vector differential operators for positions $\mathbf{r}$ and orientations $\mathbf{d}$ [73]. I_c is a binary collision integral describing short-range alignment interaction between the bacteria: direct steric collisions between the bacteria make their orientations after collision more aligned, and, consequently, more correlated [101] (see Fig. 9). In addition to collisions, bacteria interact via long-range hydrodynamic forces described by the translational and rotational velocities $\mathbf{v}$, ω. Various versions of Eqn (20) are solved directly (mostly in 2D), or reduced to a much simpler system of equations for coarse-grained quantities, such as concentration $\rho = \int P\,\mathrm{d}\mathbf{d}$ or average orientation $\tau = \int \mathbf{d}P\,\mathrm{d}\mathbf{d}$. While these kinetic models are able to reproduce some key experimental observations, like the onset of motion at some critical concentration, the agreement with experiment remains mostly qualitative.

[8] For typical experimental conditions, this torque appears to be small compared to other terms in Eqn (19).

6. Conclusions

Active colloids is a rapidly expanding and developing area, and many scientific and technological breakthroughs may occur in the near feature. One of the intriguing research avenues is the collective behavior of shape-anisotropic colloids, like rods, platelets, or even more complex shapes, e.g., chiral. Similar to liquid crystals [6], where a variety of nontrivial phases arises due to the shape anisotropy of the molecules, we can anticipate a rich spectrum of nontrivial dynamic states and structures when the suspension of anisotropic particles is energized by electric or magnetic fields. These states, showing unique optical and mechanical properties, will play a bigger role in reconfigurable smart materials for emerging technologies based on the self-assembly of anisotropic colloids, from photonics [102, 103] to microfluidic machines [62] and robotics [36, 104, 105].

Scientific breakthroughs are expected in the field of artificial swimmers. Technical progress will likely happen in the design of swimmers, optimization of their swimming abilities, and functionalization for specific applications. Current swimmer designs are based mostly on hydrogen peroxide propulsion, which makes them unsuitable for the majority of medical applications related to targeted drug delivery. The use of biologically common fuels, such as glucose, is highly desirable and promising in this respect. Another intriguing application is the design and optimization of microswimmers for specific collective tasks, like targeted cargo delivery, parallel assembly, scavenging of contaminants, and other tasks generally associated with 'swarm intelligence', an approach to the coordination of multirobot systems consisting of large numbers of simple microrobots [106].

Thanks to the revolutionary increase in computing power, a significant fidelity increase in the numerical algorithms for active colloidal suspensions is widely anticipated. The majority of current theoretical approaches are based on direct discrete particle simulations with stochastic forces due to thermal fluctuations, whereas hydrodynamic interactions are included on a highly simplified level, mostly via viscous friction acting on the particle or in the mean-field approximation (see, e.g., [58, 61, 98, 107]). A more adequate treatment of the hydrodynamic forces between colloidal particles beyond pair-wise interactions is highly desirable, but still computationally prohibitive. In addition to discrete particle simulations, a number of continuum phenomenological approaches have been proposed to describe dynamic states, like rotating binary clusters and self-propelled magnetic snakes [33, 52]. Thus, further progress is expected in the derivation of coarse-grained models for dynamic states in colloidal suspension. The models derived from the first principles, for example, in the framework of kinetic theories, should incorporate long-range forces (hydrodynamic, magnetic), as well as short range interactions (collisions, lubrications), etc.

There has been a rapidly growing number of computational and theoretical studies on the generic dynamic and statistical properties of collective behavior exhibited by self-

propelled particles with simplified interactions, from point-like particles to rigid rods and swimming flagella (see, e.g., [108–113]). A variety of dynamic phases have been predicted, including moving clusters, bands, and swarming states. However, to date, the connection between these simulations and experimentally the observed dynamics of self-propelled colloids has remained not fully satisfactorily explained. Refined computational models will likely incorporate, on a more realistic level, the specific properties of self-propelled colloids and a variety of inter-particles forces, whether electric, magnetic, steric, or hydrodynamic.

This work was supported by the U.S. Department of Energy, Office of Basic Energy Sciences, Division of Materials Science and Engineering, under Contract DEAC02-06CH11357.

References

1. Hunter R J, White L R, Chan D Y C *Foundations of Colloid Science* Vol. 1 (Oxford: Clarendon Press, 1987)
2. Norde W *Colloids and Interfaces in Life Sciences* (Boca Raton, Fla.: CRC, 2003)
3. Anscombe N, Craig F, Harris S *Eng. Technol.* **7** (2) 68 (2012)
4. Sagis L M C *Rev. Mod. Phys.* **83** 1367 (2011)
5. Frenkel D *Physica A* **313** 1 (2002)
6. Kléman M, Lavrentovich O D *Soft Matter Physics*: *an Introduction* (Berlin: Springer-Verlag, 2003)
7. Witten T A *Rev. Mod. Phys.* **71** S367 (1999)
8. Aranson I S, Tsimring L S *Granular Patterns* (Oxford: Oxford Univ. Press, 2009)
9. Israelachvili J N *Intermolecular and Surface Forces* (Burlington, MA: Academic Press, 2011)
10. Ebert F, Keim P, Maret G *Eur. Phys. J. E* **26** 161 (2008)
11. Royall C P et al. *J. Phys. Condens. Matter* **20** 404225 (2008)
12. Hiltner P A, Krieger I M *J. Phys. Chem.* **73** 2386 (1969)
13. Subramanian G et al. *Adv. Mater.* **11** 1261 (1999)
14. Hynninen A-P et al. *Nature Mater.* **6** 202 (2007)
15. Cai W, Shalaev V *Optical Metamaterials*: *Fundamentals and Applications* (Berlin: Springer-Verlag, 2009)
16. Lapine M et al. *Nature Mater.* **11** 30 (2011)
17. Miszta K et al. *Nature Mater.* **10** 872 (2011)
18. Vissers T et al. *Soft Matter* **7** 2352 (2011)
19. Vissers T et al. *J. Colloid Interface Sci.* **361** 443 (2011)
20. Leunissen M E et al. *Nature* **437** 235 (2005)
21. Leunissen M E, Vutukuri H R, van Blaaderen A *Adv. Mater.* **21** 3116 (2009)
22. Martinez-Veracoechea F J et al. *Phys. Rev. Lett.* **107** 045902 (2011)
23. Löwen H et al. *J. Phys. Condens. Matter* **17** S3379 (2005)
24. Frenkel D, Wales D J *Nature Mater.* **10** 410 (2011)
25. Löwen H *J. Phys. Condens. Matter* **20** 404201 (2008)
26. Sacanna S et al. *Nature* **464** 575 (2010)
27. Chen Q, Bae S C, Granick S *Nature* **469** 381 (2011)
28. Erb R M et al. *Nature* **457** 999 (2009)
29. Nykypanchuk D et al. *Nature* **451** 549 (2008)
30. Kraft D J et al. *Proc. Natl. Acad. Sci. USA* **109** 10787 (2012)
31. Dreyfus R et al. *Nature* **437** 862 (2005)
32. Tierno P et al. *J. Phys. Chem. B* **112** 16525 (2008)
33. Snezhko A, Belkin M, Aranson I S, Kwok W-K *Phys. Rev. Lett.* **102** 118103 (2009)
34. Kumacheva E et al. *Phys. Rev. Lett.* **91** 128301 (2003)
35. Osterman N et al. *Phys. Rev. Lett.* **103** 228301 (2009)
36. Snezhko A, Aranson I S *Nature Mater.* **10** 698 (2011)
37. Sanchez C, Arribart H, Guille M M G *Nature Mater.* **4** 277 (2005)
38. Grzybowski B A et al. *Soft Matter* **5** 1110 (2009)
39. Li F, Josephson D P, Stein A *Angew. Chem. Int. Ed.* **50** 360 (2011)
40. Snezhko A *J. Phys. Condens. Matter* **23** 153101 (2011)
41. Ebbens S J, Howse J R *Soft Matter* **6** 726 (2010)
42. Lauga E, Powers T R *Rep. Prog. Phys.* **72** 096601 (2009)
43. Gangwal S et al. *Phys. Rev. Lett.* **100** 58302 (2008)
44. Sokolov A, Aranson I S *Phys. Rev. Lett.* **103** 148101 (2009)
45. Wu X-L, Libchaber A *Phys. Rev. Lett.* **84** 3017 (2000)
46. Sokolov A, Goldstein R E, Feldchtein F I, Aranson I S *Phys. Rev. E* **80** 031903 (2009)
47. Vissers T, van Blaaderen A, Imhof A *Phys. Rev. Lett.* **106** 228303 (2011)
48. Sapozhnikov M V, Tolmachev Y V, Aranson I S, Kwok W-K *Phys. Rev. Lett.* **90** 114301 (2003)
49. Löwen H *Soft Matter* **6** 3133 (2010)
50. Aranson I S et al. *Phys. Rev. Lett.* **84** 3306 (2000)
51. Yeh S-R, Seul M, Shraiman B I *Nature* **386** 57 (1997)
52. Aranson I S, Sapozhnikov M V *Phys. Rev. Lett.* **92** 234301 (2004)
53. Sapozhnikov M V, Aranson I S, Kwok W-K, Tolmachev Y V *Phys. Rev. Lett.* **93** 84502 (2004)
54. Yethiraj A, Van Blaaderen A *Nature* **421** 513 (2003)
55. Martin J E et al. *Phys. Rev. E* **69** 021508 (2004)
56. Belkin M, Snezhko A, Aranson I S, Kwok W-K *Phys. Rev. Lett.* **99** 158301 (2007)
57. Riley N *Theor. Comput. Fluid Dyn.* **10** 349 (1998)
58. Belkin M, Glatz A, Snezhko A, Aranson I S *Phys. Rev. E* **82** 015301(R) (2010)
59. Landau L D, Lifshitz E M *Fluid Mechanics* (Oxford: Pergamon Press, 1987) [Translated from Russian: *Gidrodinamika* (Moscow: Nauka, 1986)]
60. Elsner N et al. *J. Chem. Phys.* **130** 154901 (2009)
61. Martin J E, Anderson R A, Williamson R L *J. Chem. Phys.* **118** 1557 (2003)
62. Grzybowski B A, Stone H A, Whitesides G M *Proc. Natl. Acad. Sci. USA* **99** 4147 (2002)
63. Solis K J, Bell R C, Martin J E *J. Appl. Phys.* **107** 114911 (2010)
64. Nagaoka Y, Morimoto H, Maekawa T *Langmuir* **27** 9160 (2011)
65. Smoukov S K et al. *Soft Matter* **5** 1285 (2009)
66. Paxton W F et al. *J. Am. Chem. Soc.* **128** 14881 (2006)
67. Howse J R et al. *Phys. Rev. Lett.* **99** 048102 (2007)
68. Gao W et al. *J. Am. Chem. Soc.* **133** 11862 (2011)
69. Ghosh A, Fischer P *Nano Lett.* **9** 2243 (2009)
70. Paxton W F et al. *J. Am. Chem. Soc.* **126** 13424 (2004)
71. Moran J L, Posner J D *J. Fluid Mech.* **680** 31 (2011)
72. Sanchez S et al. *J. Am. Chem. Soc.* **133** 701 (2011)
73. Kim S, Karrila S J *Microhydrodynamics. Principles and Selected Applications* (Boston: Butterworth-Heinemann, 1991)
74. Bazant M Z, Squires T M *Phys. Rev. Lett.* **92** 66101 (2004)
75. Berg H C *E. coli in Motion* (New York: Springer, 2004)
76. Dombrowski C et al. *Phys. Rev. Lett.* **93** 98103 (2004)
77. Sokolov A, Aranson I S, Kessler J O, Goldstein R E *Phys. Rev. Lett.* **98** 158102 (2007)
78. Sokolov A, Apodaca M M, Grzybowski B A, Aranson I S *Proc. Natl. Acad. Sci. USA* **107** 969 (2010)
79. Theurkauff I et al. *Phys. Rev. Lett.* **108** 268303 (2012)
80. Thakur S, Kapral R *Phys. Rev. E* **85** 026121 (2012)
81. Ke H et al. *J. Phys. Chem. A* **114** 5462 (2010)
82. Ibele M, Mallouk T E, Sen A *Angew. Chem. Int. Ed.* **48** 3308 (2009)
83. Sen A et al. *Faraday Discuss.* **143** 15 (2009)
84. Ibele M E et al. *ACS Nano* **4** 4845 (2010)
85. Cēbers A, Ozols M *Phys. Rev. E* **73** 021505 (2006)
86. Godoy M et al. *J. Appl. Phys.* **111** 044905 (2012)
87. Elfring G J, Lauga E *Phys. Rev. Lett.* **103** 088101 (2009)
88. Lambert G, Liao D, Austin R H *Phys. Rev. Lett.* **104** 168102 (2010)
89. Miño G et al. *Phys. Rev. Lett.* **106** 048102 (2011)
90. Drescher K et al. *Proc. Natl. Acad. Sci. USA* **108** 10940 (2011)
91. Drescher K et al. *Phys. Rev. Lett.* **105** 168101 (2010)
92. Hatwalne Y et al. *Phys. Rev. Lett.* **92** 118101 (2004)
93. Rafaï S, Jibuti L, Peyla P *Phys. Rev. Lett.* **104** 098102 (2010)
94. Haines B M et al. *Phys. Rev. E* **80** 041922 (2009)
95. Ryan S D et al. *Phys. Rev. E* **83** 050904(R) (2011)
96. Wysocki A, Löwen H *Phys. Rev. E* **79** 041408 (2009)
97. Aranson I S, Tsimring L S *Rev. Mod. Phys.* **78** 641 (2006)
98. Rex M, Löwen H *Eur. Phys. J. E* **26** 143 (2008)
99. Koch D L, Subramanian G *Annu. Rev. Fluid Mech.* **43** 637 (2011)
100. Saintillan D, Shelley M J *Phys. Rev. Lett.* **100** 178103 (2008)
101. Aranson I S et al. *Phys. Rev. E* **75** 040901(R) (2007)
102. Tang S K Y et al. *Adv. Mater.* **23** 2413 (2011)
103. Golovin A B, Lavrentovich O D *Appl. Phys. Lett.* **95** 254104 (2009)
104. Ilievski F et al. *Angew. Chem.* **123** 1930 (2011)

105. Donald B R et al., in *Algorithmic Foundation of Robotics VIII. Selected Contributions of the Eighth Intern. Workshop on the Algorithmic Foundations of Robotics* (Springer Tracts in Advanced Robotics, Vol. 57, Eds G S Chirikjian et al.) (Berlin: Springer-Verlag, 2010) p. 69
106. Beni G, in *Swarm Robotics. SAB 2004 Intern. Workshop, Santa Monica, CA, USA, July 17, 2004. Revised Selected Papers* (Eds E Sahin, W M Spears) (Berlin: Springer, 2005) p. 1
107. Martin J E *Phys. Rev. E* **79** 011503 (2009)
108. Grégoire G, Chaté H *Phys. Rev. Lett.* **92** 025702 (2004)
109. Ginelli F et al. *Phys. Rev. Lett.* **104** 184502 (2010)
110. Ripoll M et al. *Phys. Rev. Lett.* **101** 168302 (2008)
111. Bialké J, Speck T, Löwen H *Phys. Rev. Lett.* **108** 168301 (2012)
112. Saintillan D, Shelley M J *Phys. Rev. Lett.* **99** 58102 (2007)
113. Yang Y, Marceau V, Gompper G *Phys. Rev. E* **82** 031904 (2010)